Magnetic Properties of the Mn_5Si_3 Compound

J. Leciejewicz[a], B. Penc[b], A. Szytuła[b,*], A. Jezierski[c]
and A. Zygmunt[d]

[a]Institute of Nuclear Chemistry and Technology
Dorodna 16, 03-195 Warszawa, Poland
[b]M. Smoluchowski Institute of Physics, Jagiellonian University
Reymonta 4, 30-059 Kraków, Poland
[c]Institute of Molecular Physics, Polish Academy of Sciences
M. Smoluchowskiego 17, 60-179 Poznań, Poland
[d]W. Trzebiatowski Institute of Low Temperature and Structure Research
Polish Academy of Sciences, P.O. Box 1410, 50-950 Wrocław, Poland

Dedicated to Professor Jerzy Janik on the occasion of his 80th birthday

The magnetic and powder neutron diffraction data indicate a complex
magnetic structure of Mn_5Si_3. This compound has the hexagonal $D8_8$ crystal structure at room temperature. The Mn atoms occupy two nonequivalent sublattices. Two phase transitions, at 60 and 106 K, are observed. The first one is between a non-collinear AF1 and a collinear AF2 magnetic structure, the second one is between the collinear AF2 structure and a paramagnetic state. At 106 K the crystal structure changes from the hexagonal to the orthorhombic one. The values of the Mn magnetic moment in both structures were calculated by different *ab initio* methods. The results of the calculations are compared with the values of the Mn magnetic moment determined experimentally in this work and presented in the previous ones.

PACS numbers: 71.20.Lp, 75.25.+z, 75.50.Ee

1. Introduction

Physical properties of Mn_5Si_3 have been the subject of intensive experimental studies in detail concerning the magnetic structure. The crystal structure of Mn_5Si_3 is of the $D8_8$ type (space group $P6_3/mcm$). The manganese atoms are located in two different crystallographic sites. The atomic positions given by Aron-

*corresponding author; e-mail: szytula@if.uj.edu.pl

sson [1] are as follows: $4Mn_I$ at 4(d), $6Mn_{II}$ and 6Si at 6(g). This silicide has been reported to exhibit two phase transitions: at $T_1 \approx 66$ K and $T_2 \approx 99$ K [2–5]. Neutron diffraction measurements gave two antiferromagnetic phases: AF1 at low temperatures ($T < T_1$) and AF2 at high temperatures ($T_1 < T < T_2$) [6–11]. The data from different measurements lead to different models of the magnetic structure. Analysis of these models is presented in the discussion.

In this work new neutron diffraction and magnetic measurements were performed in purpose to explain the models of the magnetic structures of Mn_5Si_3. The obtained values of the Mn magnetic moments in different sublattices are compared with the results of *ab initio* electronic band structure calculations using different methods.

2. Experimental

The specimen of Mn_5Si_3 was prepared by a combination of induction melting and solid state diffusion techniques. The purity of the elements used was 4N for Mn and 5N for Si. The sample was melted and annealed for three days at 950°C and then quenched.

The X-ray powder diffraction analysis showed that the specimen contained only the desired hexagonal phase of the $D8_8$-type. Magnetic measurements were performed by the vibrating magnetometer in the temperature range 4.2–540 K in the external magnetic field up to 18 kOe. Neutron diffraction patterns measured in the temperature range 4.2–293 K were recorded using the DN500 powder diffractometer in the Institute of Atomic Energy — Świerk with the neutron wavelength 1.324 Å. Data processing was performed using the Fullprof program [12].

3. Results

3.1. Crystal structure

The intensities of the nuclear reflections observed in the room temperature pattern (see Fig. 1) were used for the refinement of the crystallographic parameters. The obtained results indicate that the Mn_5Si_3 compound crystallizes in the hexagonal system (the space group $P6_3/mcm$ No. 193). The Mn atoms occupy two crystallographic sites:

$$4(d): 1/3, 2/3, 0; 2/3, 1/3, 0; 1/3, 2/3, 1/2; 1/3, 1/3, 1/2,$$

and

$$6(g): x, 0, 1/4; 0, x, 1/4; \bar{x}, \bar{x}, 1/4; \bar{x}, 0, 3/4; 0, \bar{x}, 3/4; x, x, 3/4.$$

The Si atoms occupy the 6g site too, but with a different value of the x parameter. The determined values of the lattice parameters a and c are 6.917(15) Å and 4.821(8) Å while the x parameters are 0.233(3) for Mn and 0.598(4) for Si (the refinement factors are $R_{Bragg} = 2.9\%$ $R_{RF} = 3.3\%$). The crystal structure of Mn_5Si_3 and the atomic surrounding of Mn atoms at the different crystallographic sites are presented in Fig. 2.
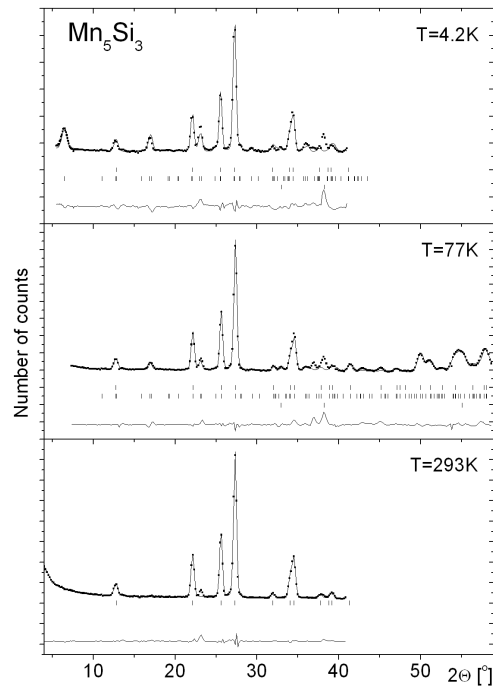
Fig. 1.   Neutron diffraction patterns of Mn₅Si₃ collected at 4.2, 77, and 293 K. The squares represent the experimental results, the solid lines are the calculated profiles for the model crystal and magnetic structures described in the text and the differences between the observed and calculated intensities (in the bottom of each diagram). The vertical bars indicate the Bragg peaks of nuclear and magnetic origin. The additional peaks at $2\theta = 23°$ and $37.2°$ correspond to the MnSi phase while the one at $38.3°$ is from the cryostat (Al).
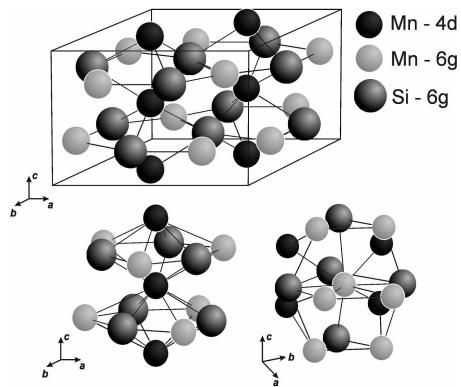
Fig. 2.   Crystal structure of Mn₅Si₃ and atom coordination polyhedral of Mn$_I$ and Mn$_{II}$.

3.2. Magnetic properties

Temperature dependence of the dc magnetic susceptibility and the reciprocal magnetic susceptibility is shown in Fig. 3. Temperature dependence of the magnetic susceptibility indicates a sharp jump at 60 K and then a rapid increase with increasing temperature. The reciprocal magnetic susceptibility obeys the
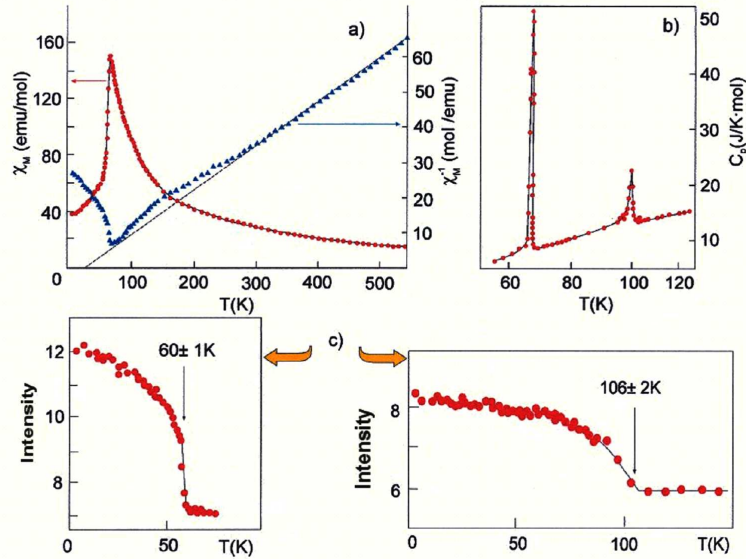
Fig. 3. Temperature dependence of the (a) dc magnetic susceptibility and the reciprocal magnetic susceptibility (the line represents the Curie–Weiss fit), (b) specific heat [2], (c) intensity of 010 (left part) and 120 and 011 (right part) magnetic peaks vs. temperature.

Curie–Weiss law above 300 K with the paramagnetic Curie temperature equal to 30 K and the average value of the effective magnetic moment equal to 3.6 μ_B. The deviation from the Curie–Weiss law observed in the temperature region 106–300 K indicates existence of a short range order above the Néel temperature.

3.3. Magnetic structure

The neutron diffraction pattern of Mn_5Si_3 recorded at 77 K shows a number of additional reflections of magnetic origin (Fig. 1). They were indexed in the orthorhombic magnetic unit cell. The parameters of this cell are connected with the hexagonal unit cell describing the crystal structure at room temperature by the following relations $a_0 \approx a_h$, $b_0 \approx \sqrt{3}b_h$, $c_0 \approx c_h$. The analysis of these peaks gives the following parameters of the magnetic unit cell $a_0 = 6.899(9)$ Å, $b_0 = 11.952(12)$ Å, and $c_0 = 4.807(4)$ Å. The distribution of the atoms in this unit cell can be described in the space group $Cmcm$ (No. 63). The Mn_I atoms occupy the 8(e) position: $x, 0, 0$ ($x = 0.333(1)$), while the Mn_{II} atoms form two

sublattices: Mn_{21} (the 4(c) sites: 0, y, 1/4 ($y = 0.239$)) and Mn_{22} (the 8(g) sites: x, y, 1/4 ($x = 0.883$, $y = x$)).

The analysis of the experimental data gives two possible models of the magnetic ordering: in the first one only the atoms in the Mn_I sublattice order antiferromagnetically. The Mn moments of 1.58(16) μ_B are located at the positions: (0, 1/3, 0), (0, 1/3, 1/2), 0, 1/6, 0) and (0, 1/6, 1/2) and are coupled ferromagnetically along the b-axis while the Mn moments at (0, 2/3, 0), (0, 2/3, 1/2), (1/2, 5/6, 0) and (1/2, 5/6, 1/2) are coupled ferromagnetically and are antiparallel to the magnetic moments of the first group. In the second model the Mn_{22} atoms have the moments equal to 1.34(14) μ_B. The spin part of the separate magnetic moments is given in Table I.

TABLE I

Values of the magnetic moments of Mn atoms at different sublattices in Mn_5Si_3 determined in powder neutron diffraction experiments at 77 and 4.2 K; different couplings between the m_x, m_y, and m_z components and total value m_{tot} of the Mn moments are shown. All values are is in μ_B; $x = 0.239$, $x' = 0.12$.

Atom	Position	77 K		4.2 K			
		m_y component		components of the Mn moments			
		Model 1	Model 2	m_x	m_y	m_z	m_{tot}
Mn_I	0 1/3 0	1.58(16)		−0.9(2)	0	−0.85(25)	1.23(25)
	0 1/3 1/2	1.58(16)		−0.9(2)		0.85(25)	1.23(25)
	1/2 1/6 0	1.58(16)		−0.9(2)		−0.85(25)	1.23(25)
	1/2 1/6 1/2	1.58(16)		−0.9(2)		0.85(25)	1.23(25)
	1/2 5/6 0	−1.58(16)		0.9(2)		0.85(25)	1.23(25)
	1/2 5/6 1/2	−1.58(16)		0.9(2)		−0.85(25)	1.23(25)
	0 2/3 0	−1.58(16)		0.9(2)		0.85(25)	1.23(25)
	0 2/3 1/2	−1.58(16)		0.9(2)		−0.85(25)	1.23(25)
Mn_{21}	0 x 1/4			−0.8(4)			−0.8(4)
	0 −x 1/4			−0.8(4)			−0.8(4)
	1/2 1/2 + x 1/4			−0.8(4)			−0.8(4)
	1/2 1/2 − x 1/4			−0.8(4)			−0.8(4)
Mn_{22}	x' x' 3/4		1.34(14)		1.63(25)		1.63(25)
	−x' −x' 1/4		1.34(14)		−1.63(25)		1.63(25)
	x' −x' 3/4		−1.34(14)		−1.63(25)		1.63(25)
	−x' x 1/4		−1.34(14)		−1.63(25)		1.63(25)
	1/2 + x' 1/2 + x' 3/4		−1.34(14)		1.63(25)		1.63(25)
	1/2 − x' 1/2 − x' 1/4		−1.34(14)		1.63(25)		1.63(25)
	1/2 + x' 1/2 − x' 3/4		1.34(14)		1.63(25)		1.63(25)
	1/2 − x' 1/2 + x' 1/4		−1.34(14)		1.63(25)		1.63(25)

An increase in the intensity of the peaks of magnetic origin and of the additional 010 peak (caused by the orthorhombic distortion) is observed in the neutron diffraction pattern collected at 4.2 K. Analysis of the intensity of these peaks leads to a complex magnetic structure (see Table I). The Mn moments at different sites form different magnetic structures. Moments at the Mn_I positions form a non-collinear antiferromagnetic structure in the *ac*-plane with the magnetic moments equal to 1.23(25) μ_B. Mn moments at the Mn_{21} and Mn_{22} sublattices form

collinear antiferromagnetic structures with the moments equal to 0.8(4) μ_B and 1.63(25) μ_B pointing along the a- and c-axis, respectively.

Figure 4 shows projections of magnetic structures on the basal plane for two models of the ordering at 77 K ((a) and (b)) and at 4.2 K (c).
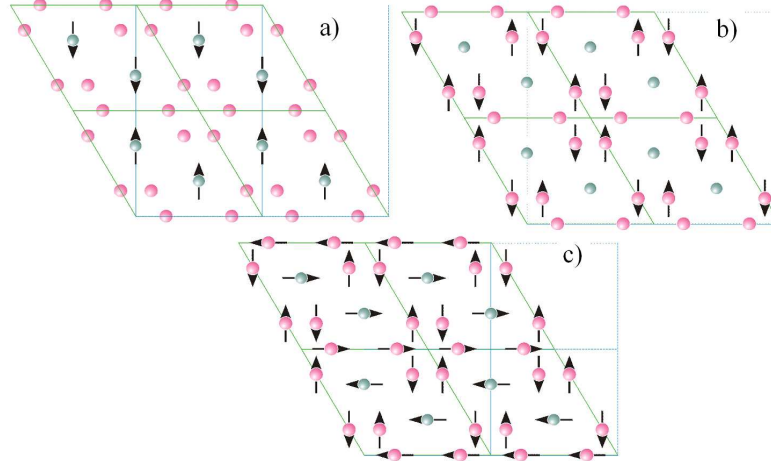
Fig. 4. The projections of magnetic structures on the basal plane for (a) model 1 and (b) model 2 at 77 K and (c) at 4.2 K (see text).

Temperature dependence of the magnetic peak intensities clearly shows two phase transitions: at 60(1) K the 010 peak disappears while the peaks 120 and 011 disappear at 106(2) K. For the 010 peak a sharp decrease in the intensity is observed at 60 K, which suggests a first-order phase transition (see Fig. 3c). These results are in agreement with the macroscopic data [3–5].

3.4. Calculation method

The electronic structure of Mn_5Si_3 was calculated using the density-functional theory within the local spin density (LSD) approximation. We applied three different *ab initio* methods: tight-binding linear-muffin tin orbital (TB LMTO) [13], Full-Potential Local-Orbital (FPLO) [14, 15] and Spin Polarized Relativistic Korringa-Kohn-Rostoker (SPR-KKR) [16, 17] for the calculation of the magnetic moments and electronic densities of states. The exchange correlation potential was assumed in the form proposed by von Barth and Hedin [18] with corrections [19] (TB LMTO), Vosko et al. [20] (SPR-KKR) and Perdew and Wang [21] (FPLO). In the TB LMTO and SPR-KKR methods the initial atomic configurations were assumed according to the periodic table of elements. In the calculation of the electronic and magnetic properties of orthorhombic Mn_5Si_3 structure by the FPLO-5 method, Mn $4s$, $4p$, $3d$, and Si $3s$, $3p$, $3d$ states were included as valence states. The $3s$, $3p$ states of Mn and $2s$, $2p$ states of Si were included as semicore states. The self-consistent calculations were performed for 486, 330 and 1221 k
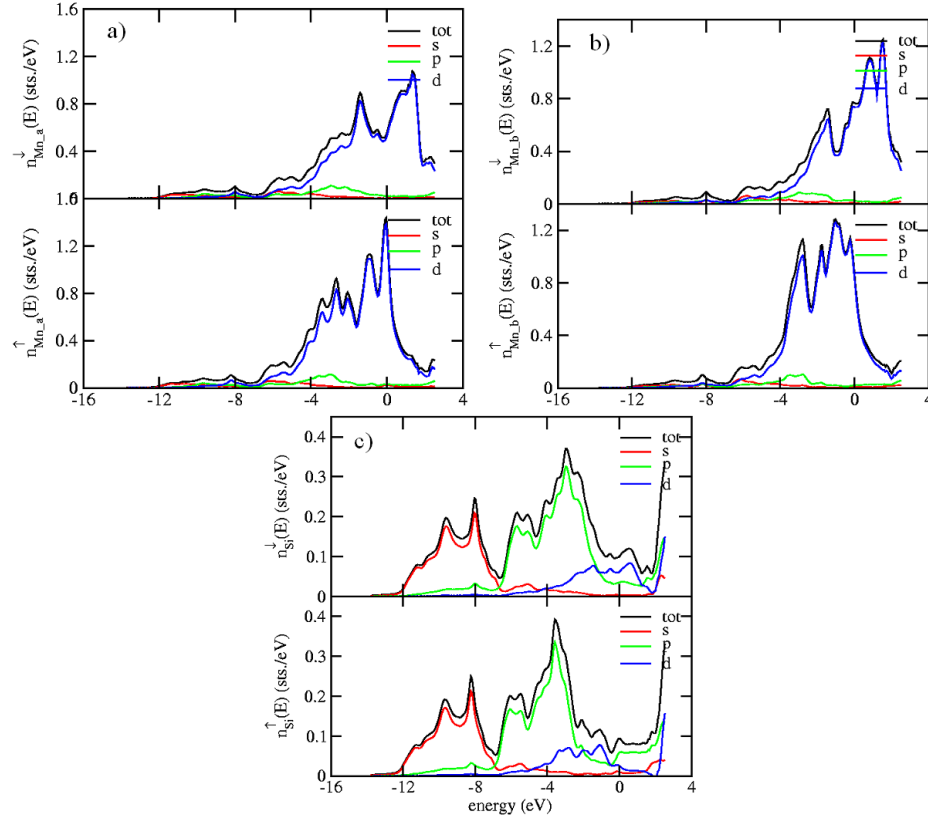
Fig. 5. Density of states calculated by the SPR-KKR-atomic spheres approximation (ASA) method for the hexagonal Mn$_5$Si$_3$. Data for: (a) Mn$_I$, (b) Mn$_{II}$, and (c) Si sublattices..

points in the irreducible wedge of the Brillouin zone for TB LMTO, SPR-KKR and FPLO method, respectively.

The calculated density of states for both Mn sites in the hexagonal crystal structure obtained by SPR-KKR method is shown in Fig. 5, while for the orthorhombic structure calculated by FPLO is plotted in Fig. 6. The electronic density of states calculated by TB LMTO method was presented in Fig. 5 of paper [22]. For both types of the crystal structure the Mn $3d$ states form the broad bands near to the Fermi level with the small shift between the states with the different orientation of spins. For the orthorhombic structure the FPLO calculations were performed for three models of the mutual ordering of the Mn moments in the Mn$_I$, Mn$_{12}$ and Mn$_{22}$ sublattices: a ferromagnetic $(+++)$ and two antiferromagnetic $(++-$ and $+-+)$ ones. The values obtained for the Mn moments are listed in Table II. For all calculations the Mn moment at the Mn$_{II}$ site is larger than the one at the Mn$_I$ site. Similar dependences between the Mn magnetic moments at different sublattices are observed in the isostructural Mn$_5$Ge$_3$ [23].

J. Leciejewicz et al.
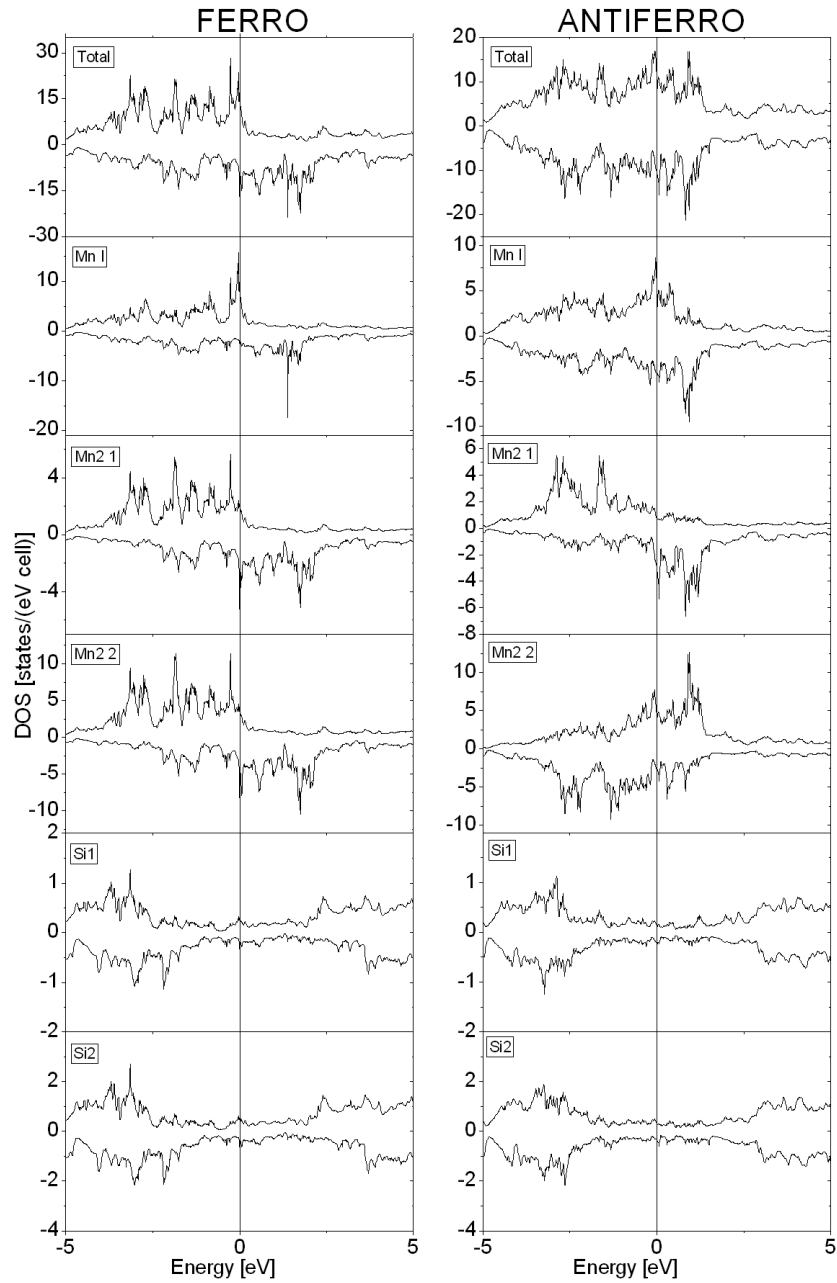
Fig. 6. Density of states calculated by FPLO method for the orthorhombic Mn_5Si_3 for ferro- and antiferro- $(++-)$ ordering between Mn sites. From the top to the bottom: total (row 1), at the three Mn sublattices (rows 2–4) and Si sublattices (rows 5 and 6).

TABLE II

Values of the magnetic moments at different Mn sublattices in Mn_5Si_3 (in μ_B).

Method/atom	Mn_I		Mn_{II}		Mn_{21}	Mn_{22}	Si		Ref.
	s	o	s	o			s	o	
SPR-KKR*	1.503	−0.023	2.339	0.026			−0.120	−0.003	this w.
FPLO*	1.545	0.007	2.734	0.028			−0.179	0.0	this w.
LMTO*	1.841		2.656				0.134		this w.
FPLO**ferro	1.46				2.53	2.64	−0.17		this w.
antiferro(++−)	0.76				2.59	1.50	0.00		this w.
antiferro(+−+)	1.49				1.91	2.29	−0.09		this w.
ND 4.2 K	0.60(6)		1.14(8)		0				[6]
ND 80 K	1.8				0.8(1)	0			[7]
ND 67 K	1.6				1.1	0.8(1)			[8]
ND 4.2 K	2.45				0	1.1			[8]
ND 66 K	0				2.30(9)	1.48			[9]
ND 4.2 K	1.20(5)				1.85(9)	0			[10]
ND 77 K	1.58(16)					or 1.34(14)			this w.
ND 4.2 K	1.23(25)				0.8(4)	1.63(25)			this w.

ND — neutron diffraction; s — spin part of the magnetic moment; o — orbital part of the magnetic moment;

*for the hexagonal structure; **for the orthorhombic structure

4. Discussion and summary

The Mn_5Si_3 compound has a hexagonal crystal structure at room temperature. The atomic surrounding of Mn atoms at different crystallographic positions are shown in Fig. 1. The Mn atoms at the 4d site have 14 neighbors ($2Mn_I$, $6Mn_{II}$, 6Si) while those at the 6g — 15 neighbors ($4Mn_I$, $6Mn_{II}$, 5Si). The interatomic distances (in Å) are listed below:

Mn_I–$2Mn_I$: 2.41 Mn_{II}–$4Mn_I$: 2.96

  –$6Mn_{II}$: 2.96   –$6Mn_{II}$: 2.87, and 2.91

  –6Si : 2.43   –5Si : 2.42, 2.48, and 2.66

With decreasing temperature the change of the crystal structure from a hexagonal to an orthorhombic one is observed at the magnetic phase transition at T_n. The orthorhombic distortion at 70 K is small (4.8×10^{-3}) and slightly changes with decreasing temperature [24]. The orthorhombic distortion causes small changes in the interatomic distances which are given below (in

Å):

Mn_I–$2Mn_I$: 2.40 Mn_{21}–Mn_{22} : 2.83

Mn_I–Si : 2.39, 2.42, 2.48 Mn_{21}–Si : 2.39, 2.42, 2.48, 2.64

     Mn_{22}–Mn_{22} : 2.82

     Mn_{22}–Si : 2.40, 2.50, 2.65

The values of the magnetic moments calculated by different methods and obtained by different authors are summarized in Table II. All models give the magnetic moments at the Mn_I site smaller than at the Mn_{II} site. Similar relation is observed for some experimental data, however the magnetic moment values

determined form the neutron diffraction data are generally smaller than the calculated ones.

The reported results indicate that all the Mn atoms carry a magnetic moment at 4.2 K. The values of the magnetic moment are different in different sublattices. At 60 K the change of the magnetic structure are observed. The magnetic data collected at 77 K lead to two possible models of the magnetic structure. In the first one the magnetic moments are localized only on the Mn_I atoms, similarly as proposed in Ref. [7]. In the second one the Mn moments are localized only on the Mn_{22} atoms.

Analysis of the interatomic distances shows that they are particularly small for Mn_I–Mn_I and Mn_I–Si indicating a strong bonding which maybe causes the decrease in the Mn magnetic moments at the Mn_I site. The suppression of the ordered moment at the Mn_I site is probably caused by the very short interatomic distance (2.40 Å) which is below the limit required for stable Mn moments. The Mn_{II}–Mn_{II} intermetallic distances are about 2.8 Å which is typical of an antiferromagnetic state.

The proposed model of the change of the magnetic structure with increasing temperature is supported by the following results of macroscopic measurements: in the temperature dependence of the magnetic susceptibility the jump at 60 K is observed (see Fig. 3b). Above this temperature the magnetic susceptibility decreases and no anomaly at the second phase transition is observed. The temperature dependence of the specific heat gives a large anomaly at 60 K while the anomaly at 100 K is about 25% of that at 60 K [2]. An anomaly in the temperature dependence of the magnetic entropy is observed only at 60 K and the second phase transition at 100 K is not detected [25].

The reported data show a good correlation between experimental and calculated values of the Mn magnetic moments at Mn_I site but not for the Mn_{II} (Mn_2 and Mn_{22}) ones. The band calculation indicates that the $3d$ electrons of the Mn_I site have rather itinerant character whereas the Mn_{21} and Mn_{22} ones are rather localized [26].

Acknowledgments

References

[1] B. Aronsson, *Acta Chem. Scand.* **14**, 1414 (1960).

[2] P.V. Geld, A.V. Mekhel'son, G.I. Kalischevich, R.P. Krentsis, Yu.V. Putinsev, N.P. Sudakova, *Sov. Phys. Solid State* **14**, 788 (1972).

[3] K.I. Meizer, R.P. Krentsis, A.A. Frolov, P.V. Geld, *Sov. Phys. Solid State* **15**, 2090 (1974).

[4] R. Haug, G. Kappel, A. Jaegle, *J. Phys. Chem. Solids* **41**, 523 (1980).

[5] R.P. Krentsis, I.Z. Radovskii, P.V. Geld, L.P. Andreeva, *Zh. Neorg. Khim.* **10**, 2192 (1965).

[6] G.H. Lander, P.J. Brown, J.B. Forsyth, *Proc. Phys. Soc.* **91**, 332 (1967).

[7] A.A. Povzner, M.E. Sheinker, R.P. Krentsis, P.V. Geld, *Izv. vuzov, Fizika* **5**, 126 (1978).

[8] A.Z. Menshikov, A.P. Vokhmyanin, Yu.A Dorofeev, *Phys. Status Solidi B* **157**, 319 (1990).

[9] P.J. Brown, J.B. Forsyth, V. Nunez, F. Tasset, *J. Phys., Condens. Matter* **4**, 10025 (1992).

[10] P.J. Brown, J.B. Forsyth, *J. Phys., Condens. Matter* **7**, 7619 (1995).

[11] A.Z. Menshikov, A.M. Balagurov, A.I. Beskrovney, A.P. Vokhmynin, D.M. Morozov, *Mater. Sci. Forum* **321-324**, 659 (2000).

[12] J. Rodriguez-Carvajal, *Physica B* **192**, 55 (1993).

[13] O.K. Andersen, O. Jepsen, *Phys. Rev. Lett.* **53**, 2571 (1984).

[14] K. Koepernik, H. Eschrig, *Phys. Rev. B* **59**, 1743 (1999).

[15] H. Eschrig, *Optimized LCAO Method and the Electronic Structure of Extended Systems*, Springer, Berlin 1989.

[16] The Munich SPRKKR package, version 3.6, H. Ebert et al., http://olymp.cup.unimuenchen.de/ak /ebert/SPRKKR.

[17] H. Ebert, in: *Fully Relativistic Band Structure Calculations for Magnetic Solid — Formalism and Application in Electronic Structure and Physical Properties of Solids*, Ed. A. Dreysse, *Lecture Notes in Physics*, Vol. 535, p. 191, Springer, Berlin.

[18] U. von Barth, L. Hedin, *J. Phys. C* **5**, 1629 (1972).

[19] D. Hu, D.C. Langreth, *Phys. Scr.* **32**, 391 (1985).

[20] S.H. Vosko, L. Wilk, M. Nusair, *Can. J. Phys.* **58**, 1200 (1980).

[21] J.P. Perdew, Y. Wang, *Phys. Rev. B* **45**, 13244 (1992).

[22] B. Penc, R. Zalecki, A. Jezierski, A. Szytuła, A. Kołodziejczyk, V. Ivanov, *Acta Phys. Pol. A* **107**, 967 (2005).

[23] B. Siberchicot, R. Henrion, J. Toboła, *Acta Phys. Pol. A* **91**, 467 (1997).

[24] Z.A. Istomina, L.P. Andreeva, S.M. Zadvorkin, A.V. Andreev, *Fizicheskie svoistva metallov i splavov*, Izd. Ural Polytechnic Institute, Svierdlovsk, 1983, p. 13 (in Russian).

[25] O. Tegus, E. Brück, L. Zhang, Dagula, K.H.J. Buschow, F.R. de Boer, *Physica B* **319**, 174 (2002).

[26] L. Vinokurova, V. Ivanov, E. Kulatov, A. Vlasov, *J. Magn. Magn. Mater.* **90-91**, 121 (1990).